



Behavior of geogrid–reinforced sand and effect of reinforcement anchorage in large-scale plane strain compression



Chia-Nan Liu ^{a,1}, Kuo-Hsin Yang ^{b,*}, Minh Duc Nguyen ^{c,2}

^a Department of Civil Engineering, National Chi-Nan University, University Road, Puli, Nantou 545, Taiwan

^b Department of Civil and Construction Engineering, National Taiwan University of Science and Technology, 43, Sec. 4, Keelung Road, Taipei 106, Taiwan

^c Department of Soil Mechanics and Foundations, University of Technical Education, Ho Chi Minh City, Viet Nam

ARTICLE INFO

Article history:

Received 10 January 2014

Received in revised form

1 July 2014

Accepted 23 July 2014

Available online 15 August 2014

Keywords:

Plane strain

Triaxial compression

Geogrid–reinforced sand

Reinforcement anchorage

ABSTRACT

This paper presents experimental investigations on the behavior of geogrid–reinforced sand featuring reinforcement anchorage which simulates the reinforcement connected to the wall facings in numerous in-situ situations. A series of large plane strain compression tests (the specimen 56 cm high × 56 cm wide × 45 cm long) was conducted. Standard Ottawa sand and 4 types of PET geogrids exhibiting 5% stiffness in the range of 750–1700 kN/m were used in this study. The specimens were tested by varying the relative density of sand, confining pressures, geogrid types, and reinforcement-anchorage conditions. Experimental results indicate that relative to unreinforced specimens, both anchored and non-anchored geogrid reinforcements can enhance the peak shear strength and suppress the volumetric dilation of reinforced soil. The studies on anchorage revealed that anchoring the reinforcement can restrain the lateral expansion of reinforced specimens, resulting in a substantial increase in shear strength and a reduction in volumetric dilation. The strength ratios of non-anchored specimens appeared to be insensitive to the reinforcement stiffness, whereas the strength ratios of the anchored specimens increased markedly with increases in soil density, reinforcement stiffness, and system deformation (*i.e.*, axial strain). Geogrid anchorage contributed a large percentage of the total shear-strength improvement, nearly 3-times more than the contribution of the soil–geogrid interaction in non-anchored specimens. Lastly, an analytical model was developed based on the concept that additional confinement is induced by reinforcement anchorage, and the predicted shear strength of the anchored soil was verified based on the experimental data.

© 2014 Elsevier Ltd. All rights reserved.

1. Introduction

Geosynthetic-reinforced soil (GRS) structures are typically composed of 4 components: soil, reinforcement, facing, and drainage. These components can mutually interact and influence the overall mechanical performance of the structure. Under numerous in-situ wall cases, reinforcements are connected to the facings of retaining walls by either frictional or mechanical approaches. In current practice, the frictional approach is applied to the segmental modular block facings by simply sandwiching the reinforcement between two blocks, and the mechanical approach is applied to cast-in-place and precast concrete facings by

mechanically connecting reinforcement to the facings. In addition to contributing to stability by mobilizing soil shear strength and reinforcing tensile strength, the facing element can help improve system stability based on its stiffness and the interaction with the reinforcement.

According to current design procedures (Elias et al., 2001; AASHTO, 2002; Berg et al., 2009; NCMA, 2009), internal stability must be evaluated to estimate the possibility of connection failure between the reinforcement layers and the facing; however, the stabilizing effects exerted by the fascia are often ignored in design procedures. Consequently, in usual design practice, it is assumed that the predicted maximum reinforcement tensile forces in each reinforcement layer are independent of the facing characteristics, and this leads to a conservative and uneconomical design of the GRS structures.

The effect of facing stiffness on the performance of reinforced soil-retaining walls was evaluated by Bathurst et al. (2006), who compared the influence of facing stiffness on the measured

* Corresponding author. Tel.: +886 2 27301227; fax: +886 2 27376606.

E-mail addresses: cnliu2009@gmail.com (C.-N. Liu), khy@mail.ntust.edu.tw (K.-H. Yang), newada119@yahoo.com (M.D. Nguyen).

¹ Tel.: +886 49 2918084; fax: +886 49 2918679.

² Tel.: +84 912327412.

reinforcement strain and reported that the wall facing is a structural element that acts to lower the magnitude of deformation, resulting in a reduction in the reinforcement strain (or load) of the GRS structures. They concluded that facing stiffness is one of the principal sources of conservatism in the current design procedures to predict the mobilized reinforcement loads. Allen et al. (2003) and Bathurst et al. (2005, 2008) proposed a working-stress method, known as the K-stiffness method, to explicitly account for the effect of facing stiffness by empirically incorporating an influence factor to increase the accuracy in predicting reinforcement tensile forces within GRS structures.

The stabilizing effects of facing elements were also considered in analytical procedures used to predict reinforcement tensile load by Klar and Sas (2009, 2010) based on the kinematic compatibility method, and by Baker and Klein (2004) and Leshchinsky et al. (1995) based on the limit equilibrium method. The results of these analytical studies suggested that the consideration of the facing element strongly affects the distribution and magnitude of reinforcement tensile loads within reinforced soil structures.

The interaction between the facing and reinforcement was discussed by Tatsuoka et al. (1989) and Tatsuoka (1992) to emphasize the importance of firmly connecting the reinforcement to the facing. Tatsuoka (1992) summarized a number of model tests exhibiting significant effects of facing rigidity on the stability of GRS walls. Tatsuoka explained that if the reinforcement and the facing were firmly connected, the active zone became highly stable as a result of the high reinforcement tensile force being mobilized, which created a high confining pressure within the active zone. A method to construct reinforced soil walls was introduced by Tatsuoka (2008); in this method, a full height rigid (FHR) facing was used and the reinforcement was firmly connected to the FHR facing. It has been demonstrated that this method can maintain high wall stability even under severe seismic conditions (Tatsuoka et al., 1998; Koseki et al., 2006).

As noted in the preceding paragraph, connecting the reinforcement to the wall facing provides several advantages that help enhance the performance and stability of reinforced soil structures. To further analyze the stress–strain–volume behavior and the strength characteristics of reinforced soil when reinforcement is connected (or anchored) to the facing, in this study, a series of large-scale plane strain compression tests was conducted on geogrid–reinforced sand, representative of soil elements inside GRS structures, in which reinforcement was anchored or not anchored. Similar approaches, the soil and the reinforcements are considered as a composite material, have also been employed in numerous studies that were conducted using triaxial compression tests (Gray and Al-Refaei, 1986; Chandrasekaran et al., 1989; Haeri et al., 2000; Zhang et al., 2006, 2008; Latha and Murthy, 2007; Tafreshi and Asakereh, 2007; Wu and Hong, 2008, 2009; Diambra et al., 2010; Chen et al., 2013; Hong and Wu, 2013; Nguyen et al., 2013), direct shear tests (Gray and Ohashi, 1983; Athanasopoulos, 1993; Farsakh et al., 2007), plane strain tests (Boyle and Holtz, 1994; Boyle, 1995; Boyle et al., 1996; Peng et al., 2000; Ketchart and Wu, 2002; Kongkitkul et al., 2007, 2008; Hou et al., 2011; Jacobs et al., 2012; Lin et al., 2013), large scale tests (Elton and Patawaran, 2004; Wu and Pham, 2013), and numerical modeling (Li et al., 2012; Lin et al., 2013); in these studies, the test variables included soil type, specimen size, confining pressure, reinforcement spacing, stiffness, strength and form, and the soil–reinforcement interface shear strength. However, only a few studies have focused on the effects of reinforcement prestressing and preloading (Roh and Tatsuoka, 2001; Lovisa et al., 2010; Lackner et al., 2013; Shivashankar and Jayaraj, 2014), and literature searches indicate that no study to date has discussed the effect of reinforcement anchorage.

In this study, the plane-strain test device allowed a geogrid layer to be anchored to both sides of a specimen box and the tensile load–elongation response of reinforcement to be monitored during the tests. Standard Ottawa sand and 4 types of PET geogrids exhibiting 5% stiffness in the range of 750–1700 kN/m were used in this study. The responses of unreinforced sand and reinforced sand in the presence and absence of reinforcement anchorage were compared. The effect of reinforcement anchorage on the shear behavior of the reinforced sand was evaluated and is discussed in this paper.

2. Experimental program

A plane-strain compression device was developed and a total of 38 plane-strain compression tests were performed. The test variables included confining pressure, relative density of sand, geogrid type, and reinforcement anchorage conditions. Furthermore, to achieve low interface frictions and to ensure that the test was conducted under plane-strain conditions, several interface treatments between sand and the steel sides of the specimen box of the test device were used.

2.1. Test device

Fig. 1a and b illustrates planar and frontal views of the large-scale plane-strain compression device used in this investigation. Fig. 1c presents the photograph of this device. This test device was developed based on the unit cell device (UCD) proposed by Boyle (1995). The large-scale plane-strain compression device used consists of a rigid specimen box made of 2-cm-thick steel plates, 2 side boxes, reaction frames, and supporting frames. In gross dimensions, the test device was 180 cm high (in 1-direction), 60 cm wide (in 2-direction), and 350 cm long (in 3-direction); the axes indicated by 1, 2, and 3 in Fig. 1 correspond to the major, intermediate (plane strain), and minor principal stress directions. The specimen box used was 56 cm high, 56 cm wide, and 45 cm long.

As indicated by Wu and Ketchart (2001), because of the complex interaction between geosynthetics and soil, a large test area is recommended for conducting tests on GRS. The geosynthetic used in this study was 33 cm wide and 45 cm long, which is sufficiently large to allow the testing of most geogrids featuring distinct patterns of apertures. The geosynthetic material was covered by 28-cm-thick soil layers on the upper and lower sides, which is sufficiently large to permit the testing of gravel up to 4.7 cm in diameter and which also satisfies the general requirement that the ratio of the minimal size of the device box to the maximal size of the soil particles should be greater than 6.0. Thus, most field soils used in reinforced earth walls and pavement construction can be tested in this device.

The vertical loading applied using a hydraulic jack was added on a rigid load plate placed on top of the soil in the specimen box. This loading system enables the loading to be applied in a tightly controlled manner during the testing, because the variation of normal load is less than 2%. Hsieh and Hsieh (2003) studied the stress distribution within a direct shear device and determined that a minimal soil thickness of 5 cm is required to ensure that uniform normal pressures are reproduced and that a concave pressure is not distributed at the shearing plane when a rigid load plate is used to apply the normal load. The size of a specimen box fulfilled this requirement completely. The system used herein can be used to apply a force up to 10 tons, which converts into 390 kPa of the vertical stress (σ_1), with the vertical deformation of specimen reaching up to 56 mm, equal to 10% of the axial strain. When the vertical load is applied, the test specimen is confined by fixed rigid plates in 2-direction, but the specimen is free to move in 3-

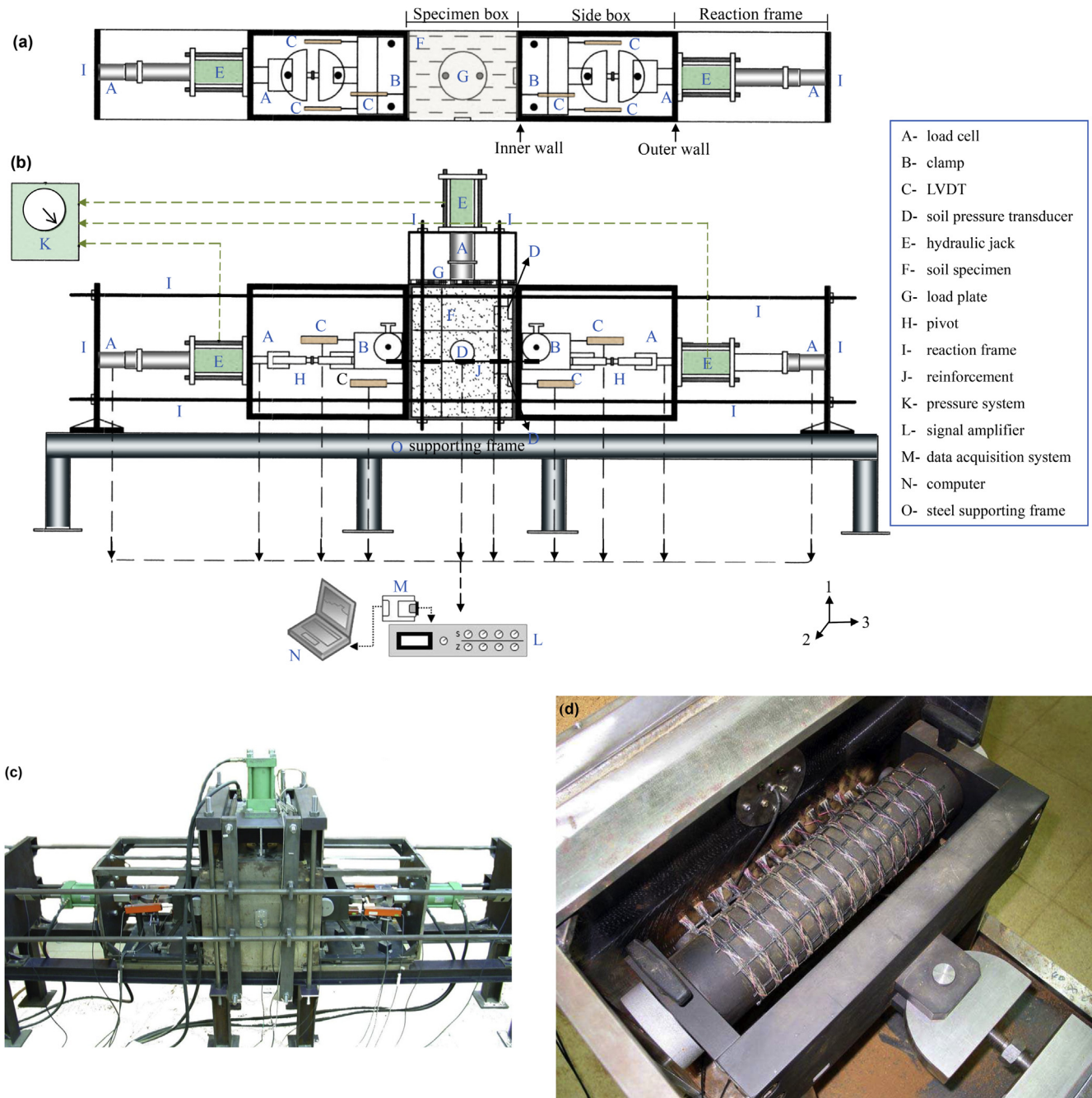


Fig. 1. The large scale plane strain compression device: (a) plane view (2–3 plane); (b) side view (1–3 plane); (c) photo; (d) details of reinforcement anchorage by roller clamps.

direction. The rigid vertical steel plates maintain the specimen in a plane-strain state during the compression test.

The 2 boxes on the 2 sides of the specimen box were composed of 2 parallel 2-cm-thick rigid steel plates connected by 4 3-cm-thick steel beams whose corners were reinforced. The bottom plates of both the side boxes rested in a low-friction, linear bearing sled that allowed the boxes free horizontal movement when the specimen expanded laterally. A constant load was applied on the outer walls of both the side boxes using hydraulic jacks. This system can be used to apply a force of up to 5 tons, which converts to 156 kPa of the lateral confining stress σ_3 . The side boxes were built adequately sturdily to preserve their rigidity when the load was applied using the hydraulic jacks.

To investigate the effect of reinforcement anchorage, geogrid reinforcement was allowed to penetrate the specimen box and enter the side box through a 33-cm-wide and 0.5-cm-high slot located at the middle of the inner wall of each side box, and the reinforcement was then gripped by roller clamps at both ends of the geosynthetic when anchored specimens were tested (Fig. 1d). Because the clamp was welded firmly to the inner wall of each side box, the mobilized reinforcement tensile load at the 2 boundaries caused by the lateral expansion of the reinforced specimen applied directly back to the reinforced specimen. These tensile loads were measured using 2 load cells connected to the 2 clamps by means of pivots. The load cells were mechanically mounted on the outer walls of the side boxes.

The forces and deformation of the soil–geosynthetic composite were measured using a set of load cells, pressure cells, and linear variable-displacement transformers (LVDTs) featuring 5-cm measuring capacity. These data were recorded and stored in the data acquisition system. The data collected during large-scale compression testing included (1) the vertical compression force applied to the specimen surface, (2) lateral confining forces applied to the specimen, (3) localized soil stresses at the side walls of the specimen box, (4) vertical compression of the specimen, (5) lateral expansion of the specimen, (6) induced tension at the 2 ends of the geosynthetic, and (7) elongation of the geosynthetic between clamps (when reinforcements were anchored during tests).

2.2. Test materials

2.2.1. Sand

The batch of Ottawa sand was used in this study. Fig. 2 presents the grain size distribution curve of the sand. The Ottawa sand has specific gravity $G_s = 2.65$, median grain size $D_{50} = 0.36$ mm, coefficient of uniformity $C_u = 1.52$, and coefficient of gradation $C_c = 0.95$; the sand is classified as poorly graded sand (SP) according to the Unified Soil Classification System (USCS). The maximum and minimum void ratios of this soil are $e_{max} = 0.76$ and $e_{min} = 0.5$, respectively. The test specimens were prepared carefully to achieve the 2 target relative densities of $D_r = 40\%$ and 80% . At $D_r = 40\%$ (loose sand), the effective shear strength parameters were $c' = 0$ and $\phi' = 35.7^\circ$ obtained from the direct shear test and $c' = 0$ and $\phi' = 42.4^\circ$ from the plane-strain compression test. At $D_r = 80\%$ (dense sand), these parameters were $c' = 0$ and $\phi' = 38.7^\circ$ from the direct shear test and $c' = 0$ and $\phi' = 45.2^\circ$ from the plane-strain compression test.

2.2.2. Geogrid

Four geogrids, denoted as GG1, GG2, GG3, and GG4, were used in this study (Fig. 3). The geogrids were woven from polyester yarns and coated with polyvinyl chloride (PVC), and they were commercial products obtained from the same manufacturer. The opening ratios (i.e., aperture area/total area) of GG1–GG4 are 61, 70, 65, and 64%, respectively. The grid patterns of GG1, GG2, GG3, and GG4 are similar, but they are dissimilar in terms of the size of aperture and in the width of rib so as to provide distinct ultimate tensile strengths in the longitudinal and transverse directions. The length and width of the specimen box were more than 15 times the maximal size of the geogrid apertures; consequently, the test area could accommodate more than 200 apertures.

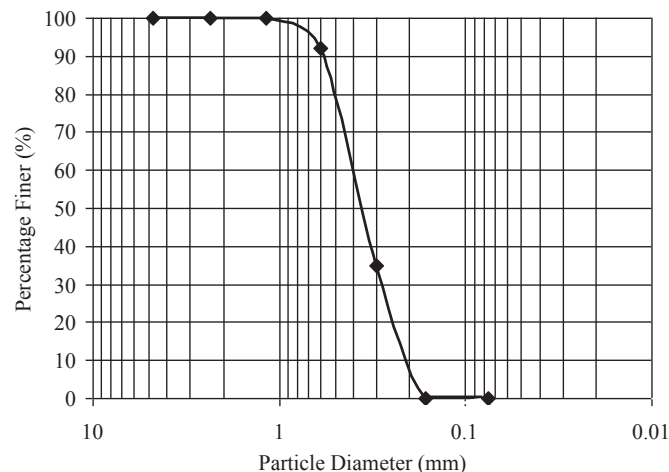


Fig. 2. Particle size distribution curve of Ottawa sand.

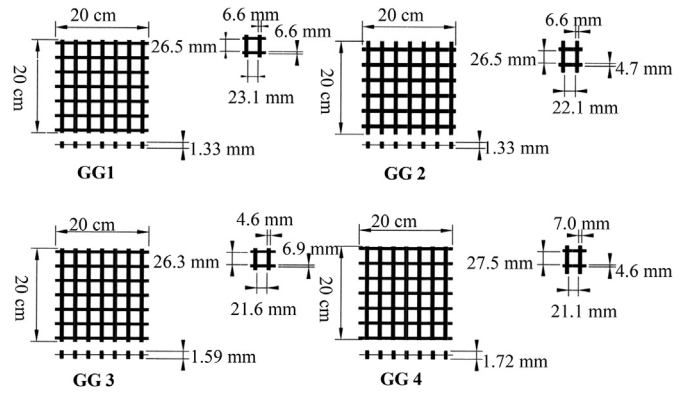


Fig. 3. Pattern and dimension of apertures of four geogrid types.

The mechanical properties of the 4 geogrids are summarized in Table 1. The load–elongation responses of the geogrids measured along the longitudinal direction in wide-width tensile tests (Fig. 4) revealed that the reinforcement stiffness ranged from small to large in the order GG1–GG4. Moreover, the sand–geogrid interface friction angles, δ_s , of loose sand were less than those of dense sand (Table 1). The disparities in δ_s among the 4 geogrids under the same soil density were small, approximately of 1° – 2° , and the δ values showed no clear relationship with the reinforcement stiffness.

2.3. Test procedure

Before placing specimens, a low-friction interface (silicon spray lubricant sandwiched between 2 layers of 0.03-mm-thick polyethylene (PE) sheets), denoted as Interface 1 in Fig. 5a, was applied on the interior walls of the specimen box to minimize the boundary resistance to the specimen during the plane-strain compression test. The details of selecting and validating this low-friction interface are presented in the next section. The specimen was prepared by tamping air-dried sand on 8 layers of 7-cm-thick sand; the layers were then compacted by using an electric vibrator on the transient surface to vibrate the steel plate that was placed on top of the soil, until the target relative densities specified for loose and dense conditions were reached.

To prepare the reinforced specimen, after completing the compaction of the initial 4 layers of soil, a layer of 33-cm-wide geogrid was positioned on top of the soil stretching out through the slots on the 2 sides of the specimen box. The reinforcement could then be either attached to the clamps on the 2 sides (called anchored specimen) or set freely (called non-anchored specimen)

Table 1
Mechanical properties of geogrids.

Property	GG1	GG2	GG3	GG4
Nominal ultimate tensile strength ^a	60 × 60	60 × 30	100 × 30	150 × 30
longitudinal × transverse (kN/m)				
Stiffness at 1% tensile strain (kN/m) ^a	687	936	1293	1795
Stiffness at 2% tensile strain (kN/m) ^a	699	891	1258	1706
Stiffness at 5% tensile strain (kN/m) ^a	703	782	1111	1528
Sand/geogrid interface friction angle	N/A	34.9	33.9	32.8
from direct shear test				
at $D_r = 40\%$, δ (degree) ^b				
Sand/geogrid interface friction angle	N/A	35.8	36.7	36.0
from direct shear test				
at $D_r = 80\%$, δ (degree) ^b				

N/A: Not available.

^a Test along the longitudinal direction according to ASTM D4595.

^b Test along the longitudinal direction according to ASTM D5321 under normal stress in the range of 50–200 kPa.

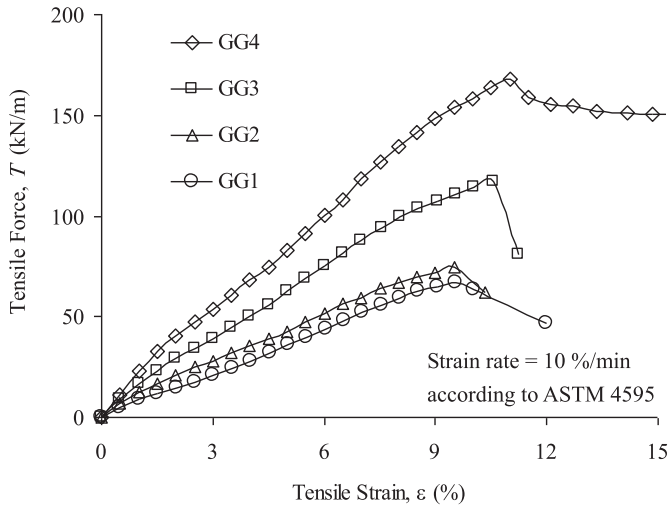


Fig. 4. Load-elongation responses of geogrids along the longitudinal direction under wide-width tensile test.

depending on the arrangement of the reinforcement (Fig. 6b and c). After placing the geogrid, the upper portion of the box was filled with soil that was compacted by following procedures identical to those used in the case of the lower portion. Subsequently, the top rigid load plate, hydraulic jacks, and reaction frames required for vertical loading and confining pressure were applied.

An automatic data acquisition system collected load and displacement data during the tests. Each specimen was initially consolidated by applying the confining pressure $\sigma_3 = 12.5, 25,$ and 50 kPa. The confining pressure applied to the specimen was measured and maintained constant in each test. After applying confining pressure, the vertical load was applied to the specimen using the load control approach with a stress rate approximately of 6 kPa/min. Because the tests were conducted by the load control instead of displacement control, test results cannot display the soil post-peak behavior. As a result, test data beyond the peak shear strength of specimen was not presented. The test was terminated when the maximal capacity of the hydraulic jacks that supplied vertical loading was reached or when the allowable displacement limits of the top side of the soil specimen were achieved.

2.4. Reduction of boundary friction

Minimizing the interface friction between the test device and the specimen is critical when performing model tests to achieve plane-strain conditions. Methods commonly employed for reducing friction resistance between the soil and the side walls include: 1. a latex rubber membrane with silicon grease, “grease method”, (Tatsuoka et al., 1984; Tatsuoka and Haibara, 1985), and 2. multiple layers of thin plastic sheeting with or without lubricant, “plastic sheet method”, (Tawfiq and Caliendo, 1993; Tognon et al., 1999; Fang et al., 2004). The plastic sheet method was adopted in this study. To quantify the effect of the proposed interface treatments on reducing the sidewall friction, a series of large-scale direct shear tests was conducted in this study on the 7 candidate interface treatments (Fig. 5a). The shearing area of the large direct shear device was 45×45 cm. The testing was performed as follows. The lower shear box was replaced with a thick steel plate on which the testing interfaces were located, and the upper shear box was filled with Ottawa sand at $D_r = 80\%$. The shearing rate was

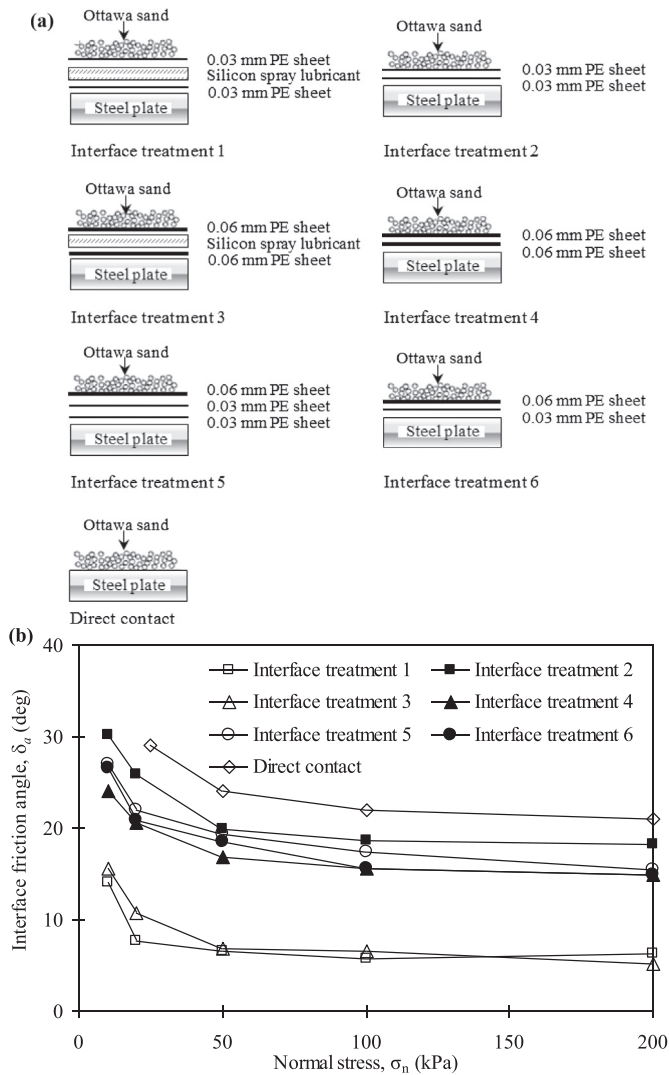


Fig. 5. Interface treatment between sand and steel sides of specimen box: (a) interface treatment profiles; (b) interface friction angle result of each interface treatment under large-scale direct shear test.

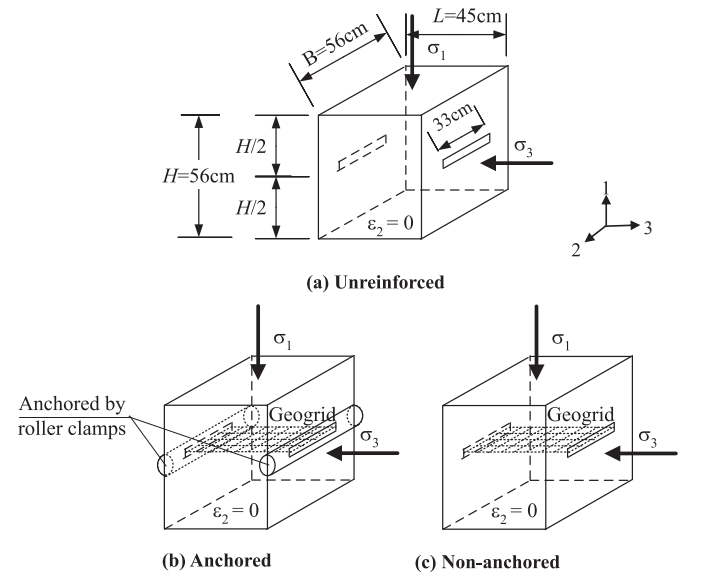


Fig. 6. Dimension and geogrid arrangement of test specimens: (a) unreinforced; (b) anchored; (c) non-anchored.

controlled to be around 10 mm/min, and the shear resistances were recorded under various applied normal stresses (10, 20, 50, 100, and 200 kPa).

Fig. 5b presents the measured interface friction angle, δ_a , of each interface treatment. The test results indicate that the interface friction angles of each interface decrease when the normal stress increases. Direct contact between sand and the steel plate created the highest interface friction angle, which ranged from 23° to 30° depending on the normal stress. The arrangements of the low-friction materials in the other 6 interfaces minimize the interface friction angle. Among these treatments, Interface 1, which consisted of a layer of silicon spray lubricant sandwiched between 2 layers of 0.03-mm PE sheets, obtained the lowest results of interface friction angle ($\delta_a \approx 6^\circ\text{--}7^\circ$ for normal stress >20 kPa). The low-friction interface induced an approximately 80% reduction in interface friction relative to the interface friction angle of the direct contact. Consequently, Interface 1 was used to create the low-friction interface in the plane-strain compression test. It should be noted that a lower boundary friction can be achieved using the grease method (approximately $\delta_a < 2^\circ$ under a normal stress > 20 kPa). However, despite possible effects of interface friction using the plastic sheet method, the main theme of this research (*i.e.*, a comparison of mechanical behavior anchored and non-anchored reinforced soil masses) should be still well identified in this paper.

3. Results and discussion

3.1. Failure pattern

Fig. 7 presents the failure pattern of unreinforced and reinforced dense specimens under $\sigma_3 = 50$ kPa. A sheet of plastic wrap was placed between the specimen and the fixed, rigid steel plates in 2-direction to trace the movement of soil particles. After dismantling the sand specimen, the developed shear band could be observed as the most intense scratch in the plastic wrap (Fig. 7). In the case of the unreinforced specimen (Fig. 7a), 2 crossing shear bands that developed in the unreinforced specimen could be clearly identified. By contrast, in the specimen reinforced using GG1 geogrid (Fig. 7b), no clear shear band was detected. This is because the geogrid placed in middle of the specimen intercepted (or restrained) the development of crossing shear bands and thereby generated a soil mass that was stronger, stiffer, and more ductile than the unreinforced soil was. This finding agrees with the results of several studies (Peng et al., 2000; Jacobs et al., 2012).

3.2. Stress–strain behavior

Stress–strain curves were obtained for geogrid–reinforced sand under anchored conditions (Figs. 8–10) and non-anchored conditions (Fig. 11). The stress–strain curves obtained for unreinforced

sand are also provided in Figs. 8–11 for the purpose of comparison. The results in these figures indicate that the shear strength of sand increased with increases in soil density and confining pressure. Compared with unreinforced sand, the soil in which geogrid was included exhibited substantially greater shear strength, in both the anchored and non-anchored specimens. Note that the anchored sand had not reached its peak shear strength even at the test limits (*i.e.*, $\sigma_1 = 390$ kPa or $\varepsilon_1 = 10\%$).

The stiffness and shear strength of anchored specimens increased substantially with increasing sand density. In the case of non-anchored sand, the shear strengths of loose specimens were lower than those of dense specimens at a low axial strain, but the strengths converged to a similar value when the axial strain was high. The use of stiffer geogrid led to higher shear strength of the anchored specimen; however, this behavior was not detected clearly in the stress–strain curves of the non-anchored specimens: when the geogrids were not anchored, similar shear strength values were measured for specimens reinforced using geogrids of varying stiffness. The effect of reinforcement anchorage is quantified and discussed later.

The shear strengths of unreinforced, non-anchored, and anchored sand were determined to differ only slightly during the initial shearing. This result indicates that during the initial shearing, the reinforcement must be deformed sufficiently to mobilize its tensile force to enhance the shear strength of the reinforced soil. The threshold values of the axial strain measured for the mobilized shear strength of reinforced sand was larger than that of unreinforced soil by approximately 2% in the case of loose specimens, and by $<1\%$ in the case of dense specimens. In this range, the reinforced soil requires larger deformation (*i.e.*, larger axial strain) to activate the effect of reinforcement when the confining pressure increases. These findings agree with the stress–strain behavior of reinforced sand determined under triaxial compression by Nguyen et al. (2013).

3.3. Volumetric strain

Figs. 8–11 show the volumetric strain responses of anchored and non-anchored specimens, respectively. The volumetric strain was calculated by $\varepsilon_v = (1 + \varepsilon_1) \times (1 + \varepsilon_3) - 1$, where the vertical strain (ε_1) and the lateral strain (ε_3 and $\varepsilon_2 = 0$) that was measured from the vertical compression and the lateral expansion using LVDTs. Soil dilation tended to increase when soil density increased and confining pressure decreased. Compared with unreinforced sand, under both anchored and non-anchored conditions, the specimens that included the reinforcement exhibited lower levels of dilation. This is because the mobilization of the tensile force in the reinforcement restrains the lateral expansion of reinforced specimens: the horizontal deformation of the sand is resisted by the applied confining pressure and the tensile loads mobilized in

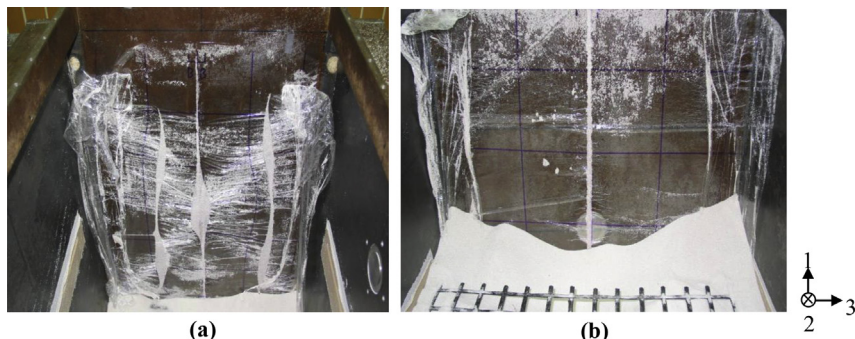


Fig. 7. Failure pattern of specimens: (a) unreinforced; (b) reinforced by GG1 geogrid (these photos were taken in 2-direction).

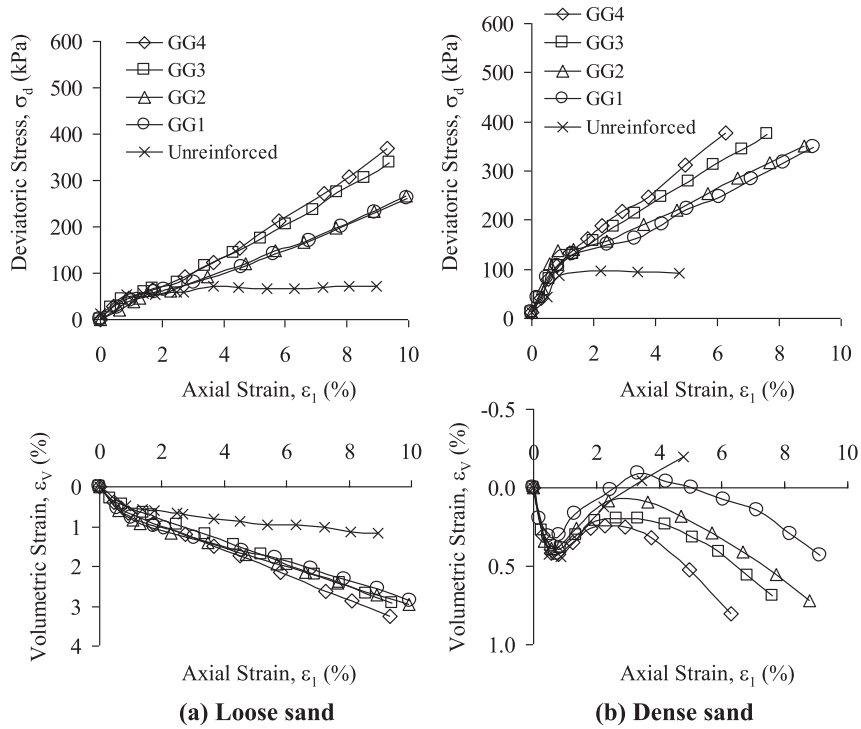


Fig. 8. Stress–strain–volumetric response of unreinforced and anchored sand under $\sigma_3 = 12.5$ kPa: (a) loose sand; (b) dense sand.

the reinforced sand specimen. The tendency to suppress the dilation in the anchored and non-anchored specimens increased with increasing reinforcement stiffness; however, distinct effects were observed in the case of dense sand under low confining pressure (Fig. 8b). The reduction of dilation due the presence of reinforcement was also observed in plane-strain tests that were conducted on non-anchored sand in several studies (Peng et al., 2000; Jacobs et al., 2012).

The suppression of soil dilation observed here, however, does not agree with the results of triaxial tests conducted on reinforced soil (Haeri et al., 2000; Nguyen et al., 2013): the reinforcement was shown to increase soil stiffness and strength, but it did not appear to suppress the dilative behavior of reinforced soil. In certain cases, the volumetric dilations of reinforced soils were measured to be even larger than those of unreinforced soils. These contrasting results obtained in triaxial tests could be misleading because, in the

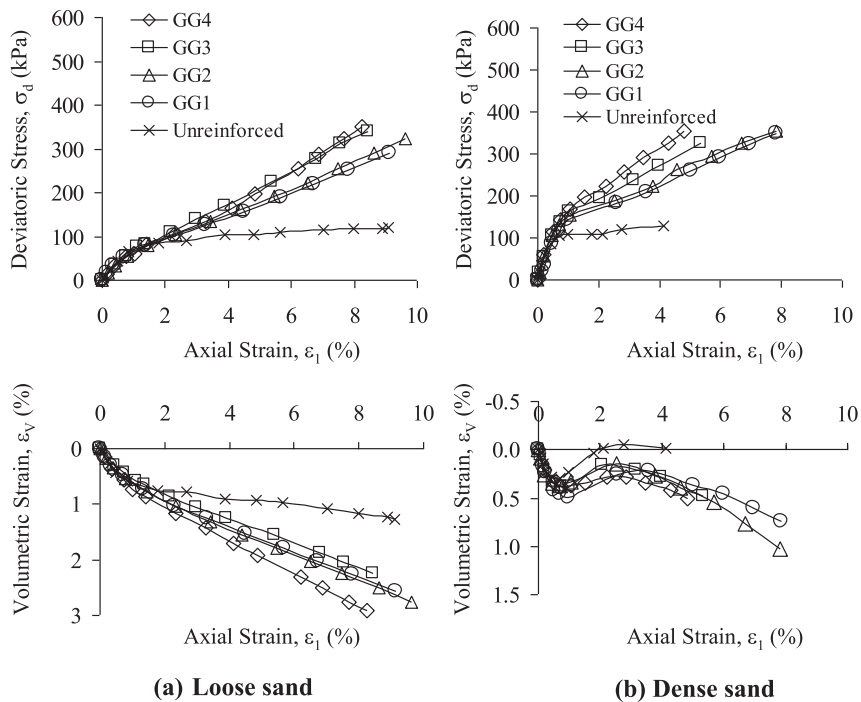


Fig. 9. Stress–strain–volumetric response of unreinforced and anchored sand under $\sigma_3 = 25$ kPa: (a) loose sand; (b) dense sand.

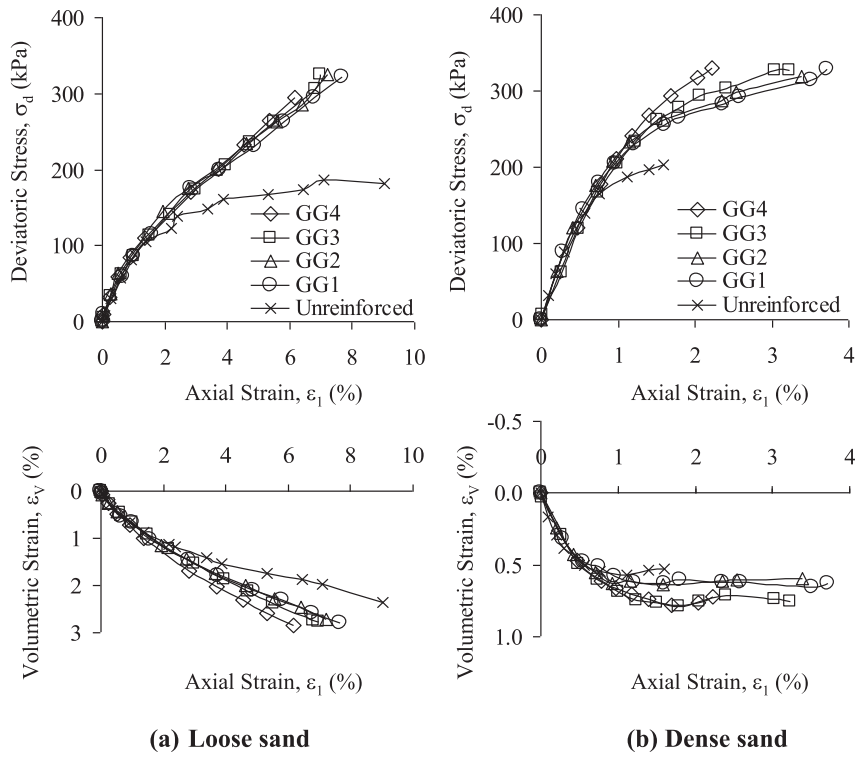


Fig. 10. Stress–strain–volumetric response of unreinforced and anchored sand under $\sigma_3 = 50$ kPa: (a) loose sand; (b) dense sand.

triaxial tests, a small specimen, typically 100 mm in diameter and 200 mm in height, was used, which differs in size compared with the specimen used in this study. The small specimen size combined with the inclusion of the geosynthetic can yield a high non-uniform soil mass and this does not represent the observed large-scale behavior of reinforced soil in the field.

3.4. Effect of reinforcement anchorage

The effect of reinforcement anchorage on stress–strain–volumetric responses is discussed in this section. Figs. 12 and 13 present comparisons of the stress–strain–volumetric responses of anchored and non-anchored specimens at $\sigma_3 = 25$ kPa. The results

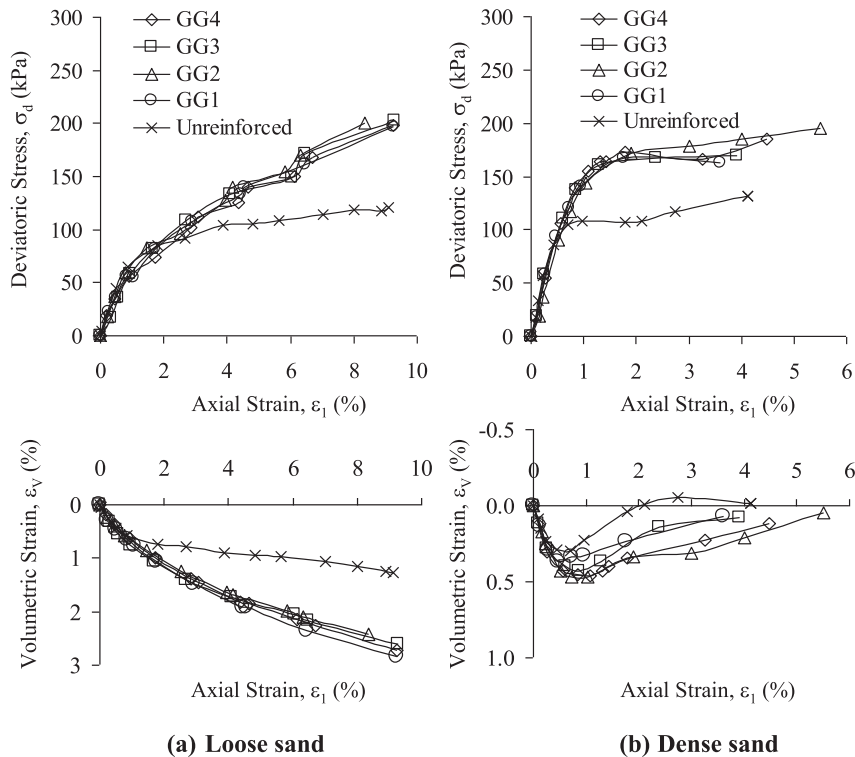


Fig. 11. Stress–strain–volumetric response of unreinforced and non-anchored sand under $\sigma_3 = 25$ kPa: (a) loose sand; (b) dense sand.

show that the specimens featuring anchored reinforcement exhibited greater shear strength than the non-anchored specimens did. The disparity in the shear strengths of anchored and non-anchored specimens increased at high axial strain, suggesting that the effect of reinforcement anchorage was enhanced when the specimen expanded laterally. This notion was validated by the measurements of the reinforcement tensile force, T_b , at the boundary (Fig. 14). The ϵ_3 given in Fig. 14 is the lateral strain of the anchored specimen, which is also equivalent to the average tensile strain of the geogrid in the longitudinal direction. Because the measured tensile forces derived from the 2 load cells located on either side of the reinforcement boundaries differed only slightly, the T_b values were averaged (Fig. 14). The results presented in Fig. 14 indicate that the mobilized reinforcement tensile load at the 2 boundaries increased when the reinforced specimen expanded laterally. This suggests that the mobilized T_b acted

directly on the reinforced specimen and concurrently induced an additional confinement on the anchored specimens and thus increased the strength and stiffness measured in the stress–strain response.

The effect of reinforcement anchorage on the volumetric strain of reinforced specimens is also presented in Figs. 12 and 13. Comparing these data with the volumetric strain of the non-anchored specimens revealed that anchoring the reinforcement effectively restrained the dilation of sand in dense specimens (Fig. 13). However, the disparity in the volumetric responses of non-anchored and anchored specimens was insignificant in loose specimens (Fig. 12). This is because loose soil tends to compress rather than dilate when sheared; consequently, the mobilized tensile force generated as a result of reinforcement anchorage becomes ineffective in volumetric suppression when the soil does not dilate.

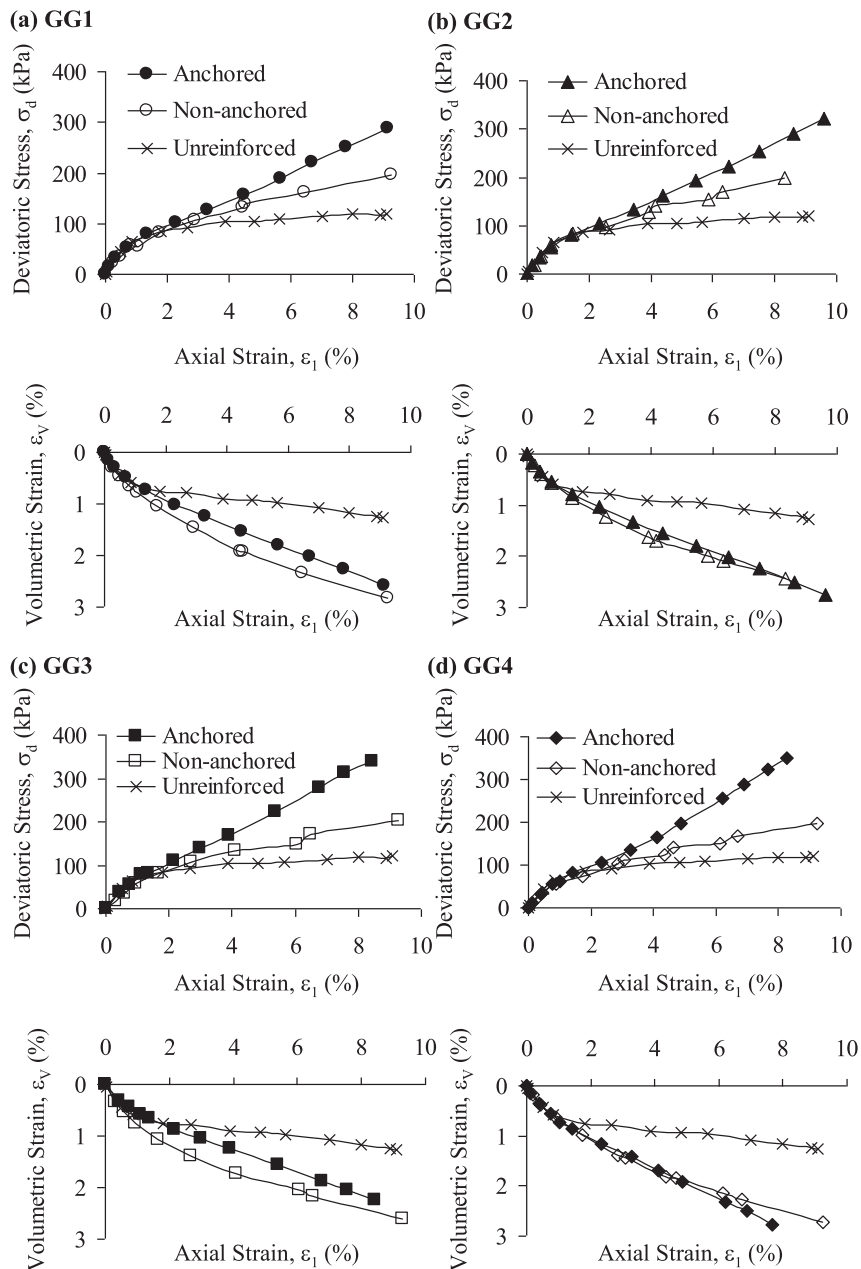


Fig. 12. Comparison of stress–strain–volumetric response among unreinforced, anchored, and non-anchored loose sand under $\sigma_3 = 25$ kPa with various geogrid types: (a) GG1; (b) GG2; (c) GG3; (d) GG4.

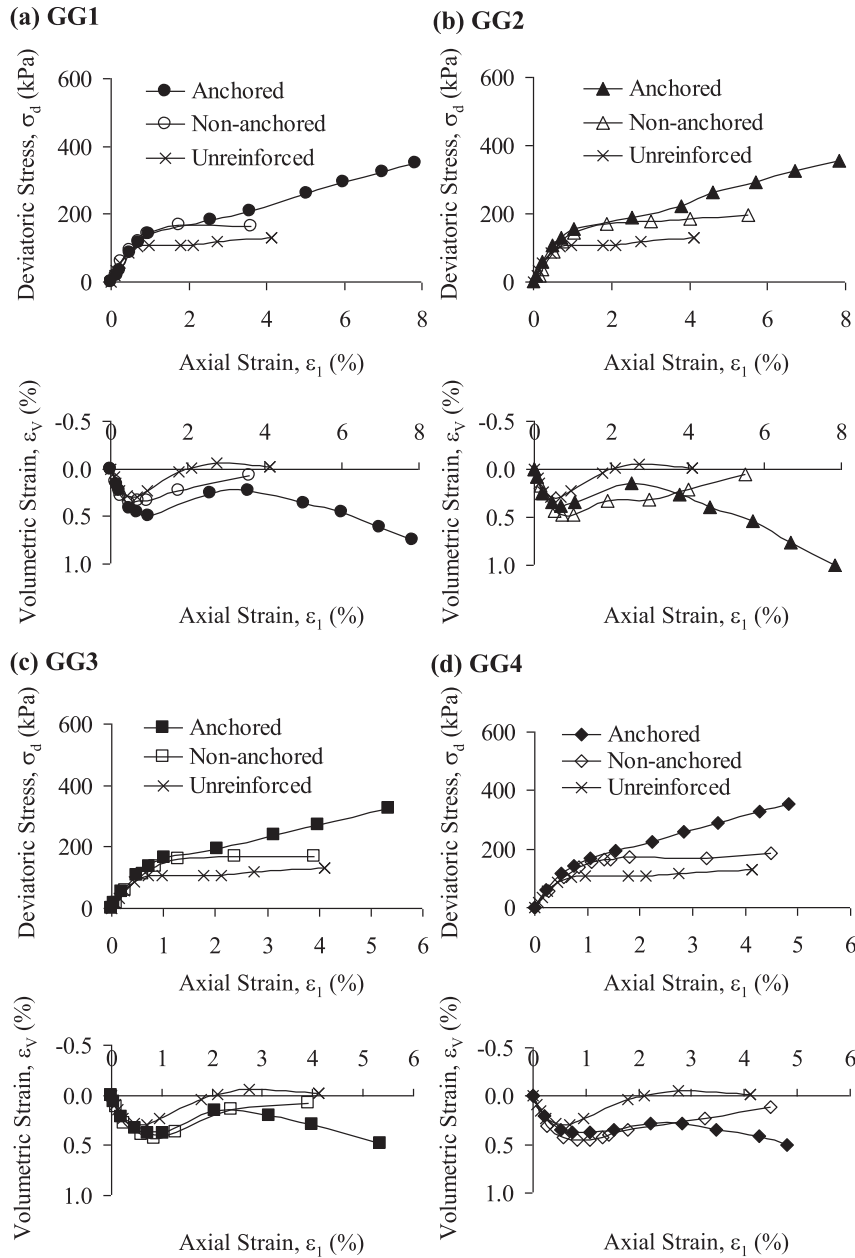


Fig. 13. Comparison of stress–strain–volumetric response among unreinforced, anchored, and non-anchored dense sand under $\sigma_3 = 25$ kPa with various geogrid types: (a) GG1; (b) GG2; (c) GG3; (d) GG4.

3.5. Strength ratio

The effect of reinforcement anchorage was further evaluated using the strength ratio (Fig. 15). The strength ratio is defined as the ratio of the deviatoric stress of reinforced specimens to that of unreinforced specimens under the same axial strain. The values of the strength ratio were evaluated under axial strains of 3% and 5%, which represent working stress and large soil-strain conditions, respectively. These strain values were chosen based on a database of 30 wall case studies (Allen et al., 2003) and the finite element studies of reinforced slopes (Yang et al., 2012; Chalaturnyk et al., 1990). In some tests of unreinforced or non-anchored dense sand, the test specimen failed before reaching 5% of axial strain. In these cases, the peak shear strength of these test specimens was selected for analysis. In general, one can observe in Fig. 15 that the strength ratio increased with an increase in soil density and

specimen deformation and became pronounced when the reinforcement was anchored. Several observations made are discussed as follows.

The dense specimens exhibited higher strength ratios than loose specimens did under the same conditions of axial strain and reinforcement stiffness and anchorage. The same conclusion is reached when comparing the strength differences between anchored loose and dense specimens (Table 2). The strength difference, $\Delta\sigma_1$, is defined as the difference in shear strength between reinforced and unreinforced soil at $\epsilon_1 = 5\%$ under the same confining pressure, which also indicates the net enhancement of strength resulting from the effects of reinforcement and anchorage. Again, the peak shear strength was selected to calculate $\Delta\sigma_1$ if the test specimen failed before reaching 5% of axial strain. Table 2 clearly shows that the value of $\Delta\sigma_1$ measured in the anchored specimen was nearly doubled when the relative density of sand was doubled.

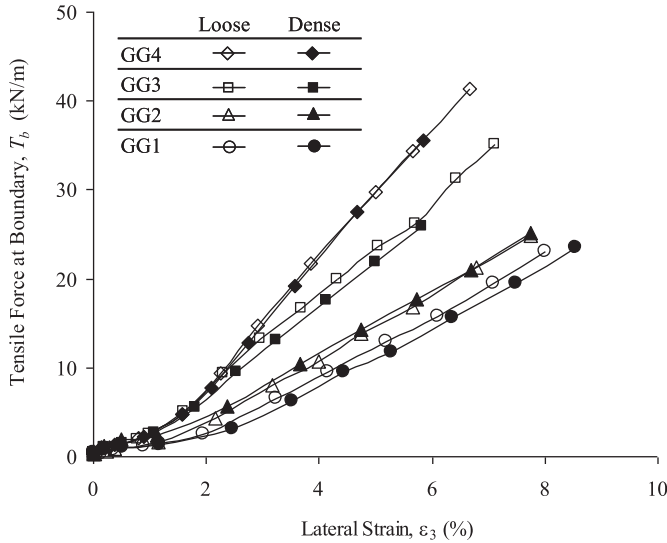


Fig. 14. Development of reinforcement tensile force measured at the boundary in the anchored specimens.

Comparing the strength-ratio values between $\epsilon_3 = 3\%$ and 5% showed that these ratios increased considerably in anchored specimens in both loose and dense specimens. This result indicates that the more the anchored specimen deforms, the greater the enhancement in shear strength caused by the mobilization of additional confinement that is induced by the reinforcement tensile loads at boundaries. However, the increasing trend in the non-anchored specimen was small in the case of loose specimens and insignificant in the case of the dense specimens, suggesting that the reinforcement that was not anchored maximally exerted its effect on shear strength improvement earlier; as shown in Fig. 13, the non-anchored dense sand reached its peak shear strength earlier before $\epsilon_1 < 5\%$.

The strength ratios of non-anchored specimens did not change markedly with an increase in reinforcement stiffness. As reported by Kongkitkul et al. (2007) and Haeri et al. (2000), the influence of other factors such as covering ratio, reinforcement unification, and sand–geotextile interface likely compensate for the reinforcing effect of reinforcement stiffness; however, these factors were not evaluated in this study. The strength ratios of both the loose and dense anchored specimens increased consistently with an increase in reinforcement stiffness (Fig. 15), suggesting that the effect of reinforcement stiffness is effectively activated when the reinforcement is anchored. The results in Table 2 also show that when the reinforcement stiffness was doubled (GG1 vs. GG4), the increments in the strength difference of the anchored loose specimens ranged from 50 to 15 kPa and decreased with an increase in confining pressure; by contrast, the increments in the case of the anchored dense specimen were approximately 100 kPa and remained nearly constant with an increase in confining pressure.

4. Analytical model

To quantify the increase in shear strength caused by reinforcement anchorage, an analytical model was developed to predict the shear strength of reinforced anchored soil. The proposed model is based on the concept that additional confinement is induced by anchoring the reinforcement at both ends. The predicted results using the proposed model were verified against the experimental test results obtained in this study.

4.1. Model concept: tensile load distribution along reinforcement

In the reinforced sand lacking anchorage (i.e., non-anchored), the outward soil–reinforcement interface shear stress, τ , mobilizes the reinforcement tensile load and then contributes to the enhancement of the shear strength of reinforced sand. Fig. 16b illustrates the typical tensile load distribution in a non-anchored sand specimen; the occurrence of the maximum tensile load, $T_{max}^{non-anchored}$, near the center of the reinforcement and that of zero load at the 2 boundaries have been reported based on the strain distribution measured in triaxial tests (Chandrasekaran et al., 1989; Nguyen et al., 2013) and plane-strain tests (Kongkitkul et al., 2008) conducted on reinforced non-anchored specimens. Based on $T_{max}^{non-anchored}$, the apparent cohesion and additional confinement approaches have been proposed to predict the shear strength of non-anchored soil (Schlosser and Long, 1974; Hausmann, 1976; Ingold and Miller, 1983; Chandrasekaran et al., 1989; Bathurst and Karpurapu, 1993; Wu and Hong, 2008; Nguyen et al., 2013).

Unlike in non-anchored specimens, in specimens that include anchored reinforcement, a substantial tensile force, T_b , is induced at the 2 boundaries of the reinforcement, and T_b increases when the anchored specimens expand laterally. Along the longitudinal direction of the reinforcement (i.e., 3-direction), the tensile force increases from the minimum value, T_b , at one boundary and reaches the peak value, $T_{max}^{anchored}$, at the middle of specimens and then reduces to T_b at the other boundary (Fig. 16c). The maximum tensile force, $T_{max}^{anchored}$, at the middle of reinforcement is equal to the sum of T_b and the extra tension mobilized as a result of the soil–reinforcement interaction. The lateral force at the specimen boundary is the combined forces obtained from σ_3 and T_b . The sole effect of reinforcement anchorage (i.e., mobilization of T_b) is analogous to the uniform distribution of tensile force in the reinforcement under wide-width tensile test conditions (Fig. 16a).

4.2. Model derivation

As discussed in the preceding subsection, an analytical model was developed based on assuming that the shear strength of anchored soil is equal to that of non-anchored soil plus the shear strength induced by reinforcement anchorage. The axial stress of anchored soil can be expressed as

$$\sigma_{1_anchored} = \sigma_{1_non-anchored} + \sigma_{3add}K_p \tag{1}$$

where $\sigma_{1_anchored}$ is the axial stress of anchored sand, $\sigma_{1_non-anchored}$ is the axial stress of non-anchored sand, σ_{3add} is the additional confining pressure induced by reinforcement anchorage, and K_p is the passive earth pressure coefficient of soil. Eq. (1) is only applied to strain levels beyond the failure strain of unreinforced soil to ensure that the limit equilibrium condition in Eq. (1) (i.e., K_p) can be held. The values of $\sigma_{1_non-anchored}$ are measured from the tests conducted on non-anchored specimens. If these tests are not available, $\sigma_{1_non-anchored}$ can be estimated using the apparent cohesion approach proposed by Schlosser and Long (1974):

$$\sigma_{1_non-anchored} = \sigma_3 K_p + 2c_a \sqrt{K_p} \tag{2}$$

where σ_3 is the confining pressure, and c_a is the apparent cohesion caused by the presence of reinforcement. Eq. (2) takes into account the increase in the shear strength of non-anchored sand caused by an apparent cohesion c_a that is generated by the reinforcement tensile forces that are induced by the development of geogrid–soil interface shear stress. The c_a values determined for loose specimens

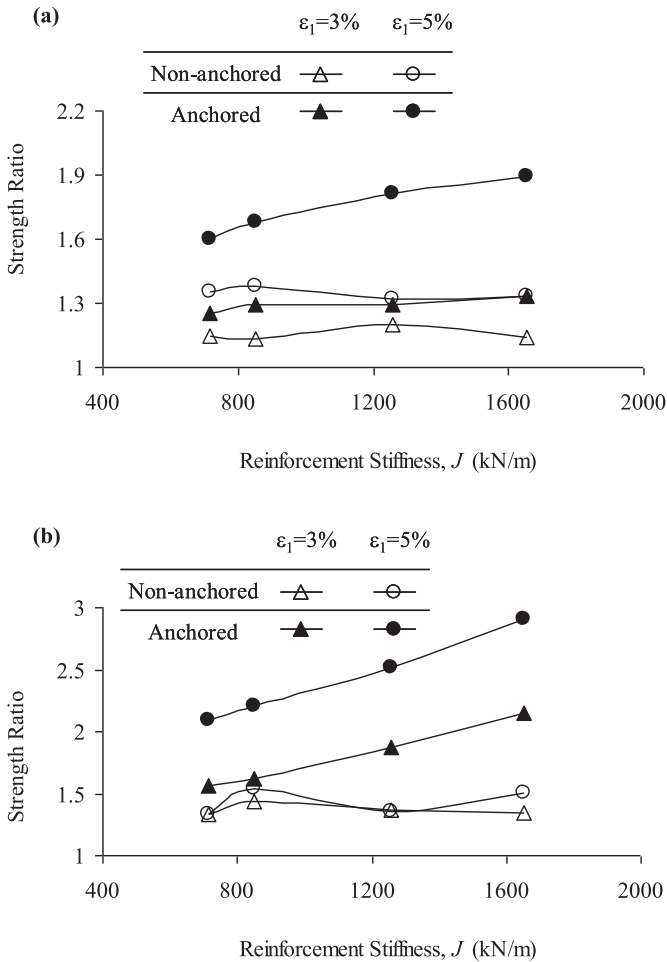


Fig. 15. Effect of reinforcement anchorage and geogrid stiffness on strength ratio at $\epsilon_1 = 3\%$ and 5% under $\sigma_3 = 25$ kPa: (a) loose sand; (b) dense sand.

reinforced by GG1–GG4 were 9.15, 8.40, 7.66, and 7.91 kN/m², and those determined for dense specimens reinforced by GG1–GG4 were 13.88, 8.54, 9.01, 12.86 kN/m², respectively. The σ_{3add} can be estimated by considering the force equilibrium of the

Table 2 Comparison of lateral strain, tensile force at the boundary and strength difference of anchored loose and dense specimens at $\epsilon_1 = 5\%$.

Geogrid	Anchored loose sand			Anchored dense sand		
	ϵ_3 (%)	T_b (kN/m)	Strength difference, $\Delta\sigma_1$ (kPa)	ϵ_3 (%)	T_b (kN/m)	Strength difference, $\Delta\sigma_1$ (kPa)
$\sigma_3 = 12.5$ kPa						
GG1	3.60	7.69	69.7	5.25	11.59	128.6
GG2	3.41	8.85	74.6	5.04	15.37	138.3
GG3	3.52	15.85	114.3	4.93	21.52	184.1
GG4	3.27	17.38	120.2	4.71	27.7	221.8
$\sigma_3 = 25$ kPa						
GG1	3.53	6.44	64.1	4.88	7.92	135.9
GG2	3.49	8.65	73.1	4.79	12.74	149.8
GG3	3.71	12.21	87.5	4.81	19.23	189.4
GG4	3.20	12.35	96.0	4.81	22.08	238.3
$\sigma_3 = 50$ kPa						
GG1	3.03	2.69	67.5	N/A		
GG2	3.04	5.75	75.3	N/A		
GG3	2.93	6.57	76.3	N/A		
GG4	2.66	7.87	81.6	N/A		

N/A: Not available because tests were forced to stop before ϵ_1 reached 5% (caused by σ_1 reaching the limit loading of device).

reinforcement tensile force at boundary, T_b , acting on the specimen box in 3-direction:

$$\sigma_{3add} = \frac{T_b l}{LH} \tag{3}$$

where l is the width of the reinforcement, and L and H are the length and height of the specimen box (Fig. 6). Combining Eqs. (1)–(3), the analytical equation derived for calculating the axial stress of anchored soil can be expressed as

$$\sigma_{1_anchored} = (\sigma_3 + \sigma_{3add})K_p + 2c_a\sqrt{K_p} \tag{4}$$

4.3. Model verification

Table 3 summarizes the measured and predicted σ_1 values of the anchored specimens using 4 types of geogrids at $\epsilon_1 = 5\%$. At the selected axial-strain level, the unreinforced sand had already reached its peak shear strength and therefore the limit equilibrium condition in Eq. (1) or (4) can be held. The results are also plotted in Fig. 17, in which the solid line is the 45° line that represents the degree of equality between the measured and predicted results. The analytical model’s predictions were accurate (followed the 45° line) in the case of the anchored loose specimens and exhibited a little scatter in the anchored dense specimens. The scatter was possibly caused by the disparity in the mobilized tensile force induced by the soil–geogrid interaction in the anchored and non-anchored dense specimens; as shown in Fig. 13, the development of volumetric strain in these specimens was different. The overall results support the conclusion that the proposed model can predict the axial stress of anchored specimens accurately ($R^2 = 0.92$). The comparative results support the assumption used in the model that the shear strength of anchored specimens is enhanced because of the combined effects of soil–geotextile interaction and reinforcement anchorage.

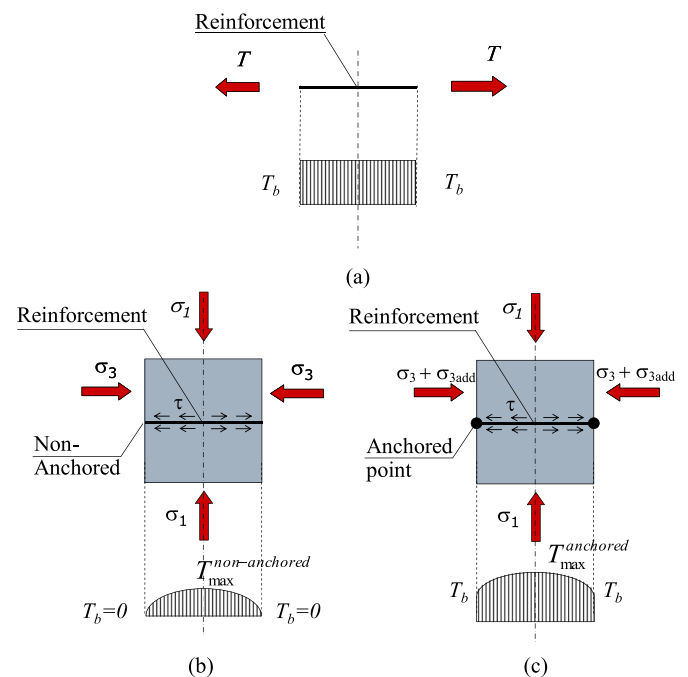


Fig. 16. Schematic illustration of tensile force distribution of reinforcements under several test conditions: (a) wide-width tensile test; (b) non-anchored sand under plane strain test; (c) anchored sand under plane strain test.

After validating the proposed model, the percentage of shear strength enhancement with respect to the unreinforced soil, which was contributed by soil–geogrid interaction and geogrid anchorage, was examined (Fig. 18). In the loose specimen, soil–geogrid interaction and geogrid anchorage exerted nearly the same effect on increasing shear strength. In the dense specimens, the geogrid anchorage contributed a large portion of the total shear strength enhancement, which was almost 3-times more than the contribution of the soil–geogrid interaction. This evaluation demonstrates the effectiveness and importance of anchoring the geogrid to increase the shear strength of reinforced soil. The shear strength can be enhanced further when high relative density is applied to the anchored sand. It should be mentioned that the discussion above is based on the test results under a constant confining pressure ($\sigma_3 = 25$ kPa). It is well known that the effect of soil–geogrid interaction becomes rather proportional to σ_3 at σ_3 lower than a certain limit. Therefore, the ratio of the shear strength improvement by geogrid anchorage to the one by geogrid/soil interaction likely increases with a decrease in σ_3 at σ_3 lower than a certain limit, suggesting that the effect of geogrid anchorage becomes more important for stabilizing soil elements closer to the wall face. The effects of σ_3 on the ratio of the shear strength improvement by geogrid anchorage to the one by geogrid/soil interaction deserve further investigation.

4.4. Stress path

Fig. 19 illustrates the stress paths of the unreinforced and reinforced specimens. In the unreinforced and non-anchored cases, the horizontal axis denotes the applied confining pressure σ_3 in the PSC test. In the anchored case, the horizontal axis indicates “the confining pressure σ_3 ” plus “the additional confinement σ_{3add} induced by reinforcement anchorage”. The effect of soil–geogrid interaction is modeled as the apparent cohesion c_a as shown in Eq. (2). The apparent cohesion approach has been adopted with an intention to emphasize the different between reinforced and unreinforced failure envelopes. It should be noted that if the additional confinement approach is also adopted to model the effect of soil–geogrid interaction, the stress paths converge to a single failure envelope irrespective of test methods (i.e. unreinforced, reinforced without anchorage, and reinforced with anchorage).

Fig. 19 shows that the stress envelope of reinforced (anchored and non-anchored) sand parallels the failure envelope of

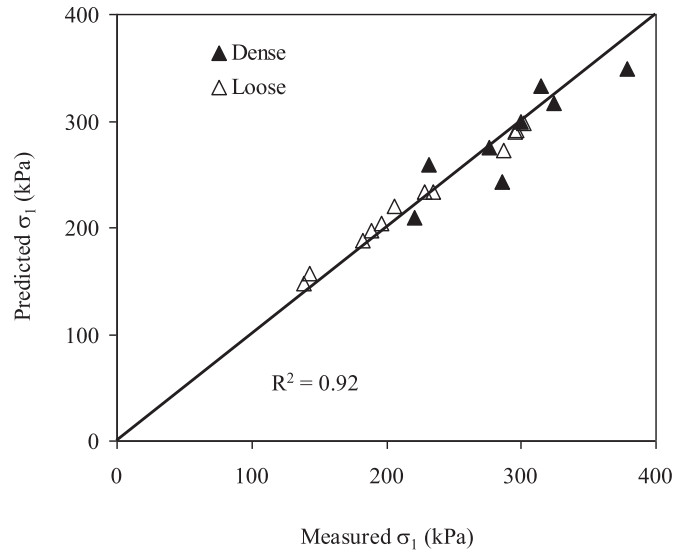


Fig. 17. Comparison between experimental and predicted axial stress of anchored sand at $\epsilon_1 = 5\%$.

unreinforced sand. The increase in the shear strength of the reinforced soil was similar to the enhancement of shear strength of unreinforced sand caused by adding a certain amount of apparent cohesion, c_a . This shear strength improvement is a result of the development of geogrid–soil interface shear stress. The presented stress envelope confirms that the apparent cohesion approach can be used to predict the shear strength of reinforced soil. Similar stress envelopes were also obtained from triaxial tests (Gray and Al-Refaei, 1986; Haeri et al., 2000) and plane-strain tests (Kongkitkul et al., 2007) in the case of reinforced non-anchored sand.

In Fig. 19, the stress paths of anchored and non-anchored specimens are used to prove that the effect of reinforcement anchorage can be modeled as the additional confinement σ_{3add} on the test specimen. Let's focus on the stress paths of anchored and non-anchored specimens at $\sigma_3 = 25$ kPa. In the case of the non-anchored specimen, the stress path rose straight up to the stress envelope of reinforced soil because the σ_3 remained constant during the test. In the case of the anchored specimen, the σ_3 increased when considering the additional confinement σ_{3add} derived using Eq. (3), which caused the stress path gradually turned right. The results in Fig. 19 show that the stress paths of the anchored and non-anchored specimens approach the same stress envelope (i.e., the stress envelope of reinforced soil in Fig. 19). The only difference is the anchored specimen reaches a higher axial stress than that of the non-anchored specimen. The key to understand the above discussion is that one can view the anchored and non-anchored soil as the same soil under different confining pressures (due to the effect of reinforcement anchorage). When subject to vertical pressures, their stress paths would converge into the same stress envelope. The soil under high confining pressure (in the case of the anchored specimen) reaches a higher shear strength (or higher axial stress) compared with that of soil under low confining pressure (in the case of the non-anchored specimen). As a result, the observation of stress paths in Fig. 19 demonstrates that the effect of reinforcement anchorage can be modeled in terms of additional confinement.

5. Conclusions

In this study, a series of large-scale plane-strain compression tests was conducted on loose and dense sand specimens that were

Table 3

Comparison of axial stress, σ_1 measured in experiments for anchored sand with the values predicted from the proposed analytical model.

Geogrid	Anchored loose sand		Anchored dense sand	
	Measured σ_1 (kPa)	Predicted σ_1 (kPa)	Measured σ_1 (kPa)	Predicted σ_1 (kPa)
$\sigma_3 = 12.5$ kPa				
GG1	143.2	156.9	230.9	255.2
GG2	138.3	147.3	221.2	205.8
GG3	182.9	187.4	276.7	269.6
GG4	188.8	196.7	314.4	326.6
$\sigma_3 = 25$ kPa				
GG1	205.5	219.5	299.4	295.8
GG2	196.5	204.4	285.4	240.0
GG3	219.9	231.8	324.0	312.4
GG4	228.4	233.6	387.8	348.7
$\sigma_3 = 50$ kPa				
GG1	296.0	291.4	N/A	
GG2	287.2	271.8	N/A	
GG3	295.0	289.1	N/A	
GG4	301.3	297.2	N/A	

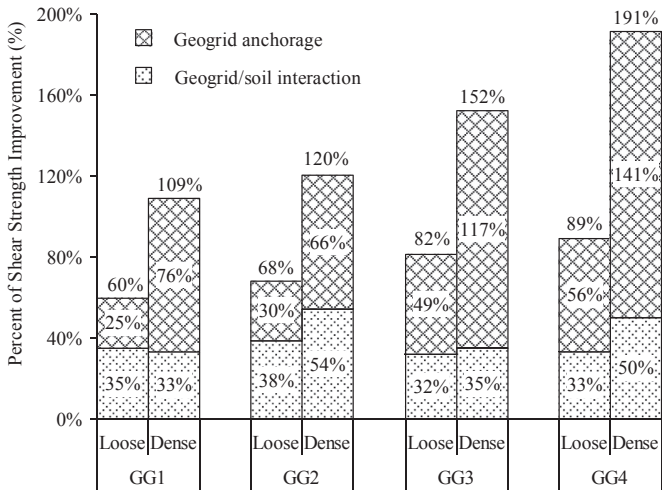


Fig. 18. Comparison of percentage of shear strength improvement contributed by soil/geogrid interaction and geogrid anchorage for different geogrids at $\epsilon_1 = 5\%$ and $\sigma_3 = 25$ kPa.

reinforced using 4 types of geogrids. The geogrid was anchored at both ends as a method to improve the performance of the reinforced soil. The main goal in this study was to investigate the effect of reinforcement anchorage on the behavior of reinforced sand. The conclusions of this study are the following.

1. Geogrid inclusion in both anchored and non-anchored specimens improves stress–strain–volumetric performance by increasing the peak shear strength and axial strain at failure of specimens. Moreover, geogrid inclusion suppresses volumetric dilation in the reinforced dense specimens.
2. Anchoring the geogrid at both ends can restrain the lateral expansion of reinforced specimens, which provides several advantages over non-anchored sand, such as substantial shear strength enhancement and reduced volumetric dilation. Combining the high stiffness of geogrid with the high relative density of soil improves the effectiveness of shear strength enhancement in the case of anchored sand.
3. The strength ratios of both the loose and dense anchored specimens increase consistently with the increase in reinforcement stiffness, suggesting that the effect of reinforcement stiffness is activated effectively when the reinforcement is anchored. However, the enhancement of the shear strength of

non-anchored specimens appears to be insensitive to reinforcement stiffness.

4. Because of geogrid anchorage, the tensile force at the geogrid boundaries is mobilized and it creates the reaction force in the form of an additional confining pressure that directly applies back to the reinforced specimen. This study validates the proposed analytical model based on assuming that the shear strength of anchored soil is the combination of the strength of non-anchored soil resulting from the soil–geogrid interaction and that induced by the additional confining pressure caused by reinforcement anchorage.
5. Soil–geogrid interaction and geogrid anchorage increase shear strength nearly equally in the loose specimen, whereas in the dense specimens, geogrid anchorage contribute a large portion of the total shear-strength enhancement, almost 3-times more than the contribution of the soil–geogrid interaction. This result demonstrates the effectiveness and importance of anchoring the geogrid in enhancing the shear strength of reinforced soil.

Notation

The following symbols are used in this paper. Basic SI units are given in parentheses.

- B width of specimen box (m)
- c_a apparent cohesion (Pa)
- C_u coefficient of uniformity (dimensionless)
- C_c coefficient of gradation (dimensionless)
- D_{50} median grain size (m)
- D_r relative density (dimensionless)
- e_{max}, e_{min} maximum and minimum void ratios respectively (dimensionless)
- G_s specific gravity of soil (dimensionless)
- H height of specimen box (m)
- J secant stiffness of geotextile (N/m)
- K_p passive earth pressure coefficient (dimensionless)
- l width of reinforcement (m)
- L length of specimen box (m)
- R^2 coefficient of determination (dimensionless)
- T tensile force in geotextile (N)
- T_b measured reinforcement tensile force at the boundary (N)
- $T_{max}^{non-anchored}, T_{max}^{anchored}$ maximum tensile load of reinforcement in non-anchored sand and in anchored sand respectively (N)
- ϵ tensile strain of reinforcement (dimensionless)
- $\epsilon_1, \epsilon_2, \epsilon_3$ and ϵ_v axial strain in axes 1, 2 and 3 and volumetric strain of specimens respectively (dimensionless)
- σ_1, σ_3 vertical stress and confining pressure respectively (Pa)
- $\sigma_{1-anchored}, \sigma_{1-non-anchored}$ axial stress of anchored and non-anchored sand respectively (Pa)
- σ_{3add} additional confining pressure due to reinforcement anchorage (Pa)
- σ_d deviatoric stress (Pa)
- $\Delta\sigma_1$ strength difference (Pa)
- ϕ' effective friction angle of soil (degree)
- δ, δ_a interface friction angle between soil–geotextile interface and soil-treated side of specimen box interface respectively
- τ interface shear stress (Pa)

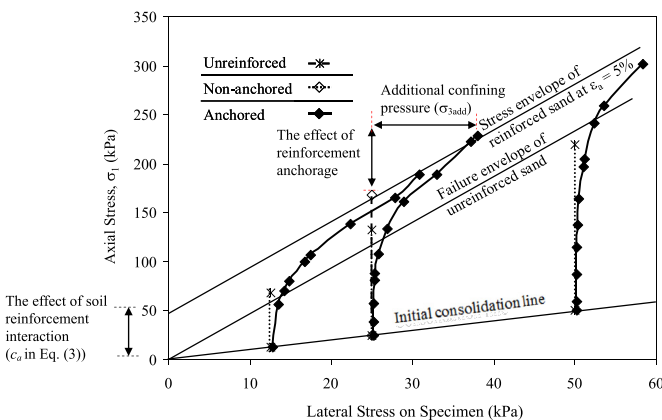


Fig. 19. Stress paths of unreinforced, non-anchored and anchored loose sand specimens reinforced by GG4 under different confining pressures.

References

AASHTO, 2002. Standard Specifications for Highway Bridges, 17th ed. American Association of State Highway and Transportation Officials (AASHTO), Washington, DC, USA.

- Allen, T.M., Bathurst, R.J., Holtz, R.D., Walters, D., Lee, W.F., 2003. A new working stress method for prediction of reinforcement loads in geosynthetic walls. *Can. Geotech. J.* 40 (5), 976–994.
- ASTM D4595. Standard Test Method for Tensile Properties of Geotextiles by the Wide-width Strip Method. ASTM International, West Conshohocken, PA, USA.
- ASTM D5321. Standard Test Method Determining the Shear Strength of Soil-geosynthetic and Geosynthetic-geosynthetic Interfaces by Direct Shear. ASTM International, West Conshohocken, PA, USA.
- Athanasopoulos, G.A., 1993. Effect of particle size on the mechanical behaviour of sand–geotextile composites. *Geotext. Geomembr.* 12 (3), 255–273.
- Baker, R., Klein, Y., 2004. An integrated limiting equilibrium approach for design of reinforced soil retaining structures, part 1 – formulation. *Geotext. Geomembr.* 22 (3), 119–150.
- Bathurst, R.J., Allen, T.M., Walters, D.L., 2005. Reinforcement loads in geosynthetic walls and the case for a new working stress design method. *Geotext. Geomembr.* 23 (4), 287–322.
- Bathurst, R.J., Karpurapu, R., 1993. Large-scale triaxial compression testing of geocell reinforced granular soils. *Geotech. Test. J. ASTM* 16 (3), 293–303.
- Bathurst, R.J., Miyata, Y., Nernheim, A., Allen, T.M., 2008. Refinement of K-stiffness method for geosynthetic reinforced soil walls. *Geosynth. Int.* 15 (4), 269–295.
- Bathurst, R.J., Vlachopoulos, N., Walters, D.L., Burgess, P.G., Allen, T.M., 2006. The influence of facing stiffness on the performance of two geosynthetic reinforced soil retaining walls. *Can. Geotech. J.* 43 (12), 1225–1237.
- Berg, R., Christopher, B.R., Samtani, N., March 2009. Design of Mechanically Stabilized Earth Walls and Reinforced Soil Slopes, vols. I and II. National Highway Institute, Federal Highway Administration, Washington, D.C. Report No. FHWA-NHI-10-024.
- Boyle, S.R., 1995. Unit cell tests on reinforced cohesionless soils. In: *Proceedings of Geosynthetics'95*, IFAI, 3, Nashville, TN, USA, February 1995, pp. 1221–1234.
- Boyle, S.R., Gallagher, M., Holtz, R.D., 1996. Influence of strain rate, specimen length and confinement on measured geotextile properties. *Geosynth. Int.* 3 (2), 205–225.
- Boyle, S.R., Holtz, R.D., 1994. Deformation characteristics of geosynthetics-reinforced soil. In: *Proceedings of the 5th International Conference on Geotextiles, Geomembranes and Related Products*, Singapore, September 1994, pp. 361–364.
- Chalaturnyk, R.J., Scott, J.D., Chan, D.H.K., Richards, E.A., 1990. Stresses and deformations in a reinforced soil slope. *Can. Geotech. J.* 27 (2), 224–232.
- Chandrasekaran, B., Broms, B.B., Wong, K.S., 1989. Strength of fabric reinforced sand under axisymmetric loading. *Geotext. Geomembr.* 8 (4), 293–310.
- Chen, R.H., Huang, Y.W., Huang, F.C., 2013. Confinement effect of geocells on sand samples under triaxial compression. *Geotext. Geomembr.* 37, 35–44.
- Diambra, A., Ibraim, E., Muir Wood, D., Russell, A.R., 2010. Fibre reinforced sands: experiments and modeling. *Geotext. Geomembr.* 28 (3), 238–250.
- Elias, V., Christopher, B.R., Berg, R.R., 2001. Mechanically Stabilized Earth Walls and Reinforced Soil Slopes Design and Construction Guidelines. Report No. FHWA-NHI-00-043. National Highway Institute, Federal Highway Administration, Washington, D.C.
- Elton, D.J., Patawaran, M.A.B., 2004. Mechanically Stabilized Earth Reinforcement Tensile Strength from Tests of Geotextile-reinforced Soil. *Transportation Research Record* 1868. Transportation Research Board, Washington, DC, pp. 81–88.
- Fang, Y.S., Chen, T.J., Holtz, R.D., Lee, W.F., 2004. Reduction of boundary friction in model tests. *Geotech. Test. J. ASTM* 27 (1), 3–12.
- Farsakh, M.A., Coronel, J., Tao, M.J., 2007. Effect of soil moisture content and dry density on cohesive soil–geosynthetic interactions using large direct shear tests. *J. Mater. Civ. Eng.* 19 (7), 540–549.
- Gray, D.H., Ohashi, H., 1983. Mechanics of fiber reinforcement in sand. *J. Geotech. Eng. ASCE* 109 (3), 335–353.
- Gray, D.H., Al-Refeai, T., 1986. Behavior of fabric vs. fiber reinforced sand. *J. Geotech. Eng. ASCE* 112 (8), 804–820.
- Haeri, S.M., Noorzad, R., Oskoorouchi, A.M., 2000. Effect of geotextile reinforcement on the mechanical behavior of sand. *Geotext. Geomembr.* 18 (6), 385–402.
- Hausmann, M.R., 1976. Strength of reinforced soil. In: *Proc. 8th Aust. Road. Res. Conf.* pp. 1–8, 8(13).
- Hsieh, C., Hsieh, M.W., 2003. Load plate rigidity and scale effects on the frictional behavior of sand/geomembrane interfaces. *Geotext. Geomembr.* 21 (1), 25–47.
- Hong, Y.S., Wu, C.S., 2013. The performance of a sand column internally reinforced with horizontal reinforcement layers. *Geotext. Geomembr.* 41, 36–49.
- Hou, J., Zhang, M.X., Zhou, H., Javadi, A.A., Peng, M.Y., 2011. Experiment and analysis of strength behavior of soil reinforced with horizontal-vertical inclusions. *Geosynth. Int.* 18 (4), 150–158.
- Ingold, T.S., Miller, K.S., 1983. Drained axisymmetric loading of reinforced clay. *J. Geotech. Eng. ASCE* 109 (7), 883–898.
- Jacobs, F., Ruiken, A., Ziegler, M., 2012. Experimental investigation of geogrid reinforced soil under plane strain conditions. In: *Proc. 5th Asian Regional Conference on Geosynthetics*, Bangkok, Thailand, pp. 823–829.
- Ketchart, K., Wu, J.T.H., 2002. A modified soil-geosynthetic interactive performance test for evaluating deformation behavior of GRS structures. *Geotech. Test. J.* 25 (4), 405–413.
- Klar, A., Sas, T., 2009. Rational approach for the analysis of segmental reinforced soil walls based on kinematic constraints. *Geotext. Geomembr.* 27 (5), 332–340.
- Klar, A., Sas, T., 2010. The KC method: numerical investigation of a new analysis method for reinforced soil walls. *Comput. Geotech.* 37, 351–358.
- Kongkitkul, W., Hirakawa, D., Tatsuoka, F., Kanemaru, T., 2007. Effects of geosynthetic reinforcement type on the strength and stiffness of reinforced sand in plane strain compression. *Soil. Found.* 47 (6), 1109–1122.
- Kongkitkul, W., Hirakawa, D., Tatsuoka, F., 2008. Residual deformation of Geosynthetic-reinforced sand in plane strain compression affected by viscous properties of geosynthetic reinforcement. *Soil. Found.* 48 (3), 333–352.
- Koseki, J., Bathurst, R.J., Guler, E., Kuwano, J., Maugeri, M., 2006. Seismic stability of reinforced soil walls, Keynote lecture. In: *Proc. 8th International Geosynthetics Conference (8ICG)*, Yokohama, pp. 51–77.
- Lackner, C., Bergado, D.T., Semprich, S., 2013. Prestressed reinforced soil by geosynthetics – concept and experimental investigation. *Geotext. Geomembr.* 37, 109–123.
- Latha, G.M., Murthy, V.S., 2007. Effects of reinforcement form on the behavior of geosynthetic reinforced sand. *Geotext. Geomembr.* 25 (1), 23–32.
- Leshchinsky, D., Ling, H., Hanks, G., 1995. Unified design approach to geosynthetic reinforced slopes and segmental walls. *Geosynth. Int.* 2 (5), 845–881.
- Li, F.L., Peng, F.L., Tan, Y., Kongkitkul, W., Siddiquee, M.S.A., 2012. FE simulation of viscous behavior of geogrid-reinforced sand under laboratory-scale plane-strain-compression testing. *Geotext. Geomembr.* 31, 72–80.
- Lin, Y.L., Zhang, M.X., Javadi, A.A., Lu, Y., Zhang, S.L., 2013. Experimental and DEM simulation of sandy soil reinforced with H–V inclusions in plane strain tests. *Geosynth. Int.* 20, 161–173.
- Lovisa, J., Shukla, S.K., Sivakugan, N., 2010. Behaviour of prestressed geotextile-reinforced sand bed supporting a loaded circular footing. *Geotext. Geomembr.* 28 (1), 23–32.
- NCMA, 2009. In: Bernardi, M. (Ed.), *Design Manual for Segmental Retaining Walls*, third ed. National Concrete Masonry Association, Herndon, VA, USA.
- Nguyen, M.D., Yang, K.H., Lee, S.H., Wu, C.S., Tsai, M.H., 2013. Behavior of nonwoven geotextile-reinforced soil and mobilization of reinforcement strain under triaxial compression. *Geosynth. Int.* 20 (3), 207–225.
- Peng, F.L., Kotake, N., Tatsuoka, F., Hirakawa, D., Tanaka, T., 2000. Plane strain compression behaviour of geogrid-reinforced sand and its numerical analysis. *Soil. Found.* 40 (3), 55–74.
- Roh, H.S., Tatsuoka, F., 2001. Effects of preloading and prestressing on the strength and stiffness of geosynthetic-reinforced clay in plane strain compression. *Geosynth. Int.* 8 (5), 393–444.
- Schlosser, F., Long, N.T., 1974. Recent results in French research on reinforced earth. *J. Const. Div. Proc. ASCE* 100 (3), 223–237.
- Shivashankar, R., Jayaraj, J., 2014. Effects of prestressing the reinforcement on the behavior of reinforced granular beds overlying weak soil. *Geotext. Geomembr.* 42 (1), 69–75.
- Tafreshi, S.N.M., Asaker, A., 2007. Strength evaluation of wet reinforced silty sand by triaxial test. *Int. J. Civ. Eng.* 5 (4), 274–283.
- Tatsuoka, F., 1992. Roles of facing rigidity in soil reinforcing. In: *Keynote Lecture. Proc. Earth Reinforcement Practice*, Fukuoka, Japan, vol. 2, pp. 831–870.
- Tatsuoka, F., 2008. Recent practice and research of geosynthetic-reinforced earth structures in Japan. *J. Geoenviron. Eng.* 3 (3), 77–100.
- Tatsuoka, F., Haibara, O., 1985. Shear resistance between sand and smooth or lubricated surface. *Soil. Found.* 25 (1), 89–98.
- Tatsuoka, F., Molenkamp, F., Torii, T., Hino, T., 1984. Behavior of lubrication layers of foundations in element tests. *Soil. Found.* 24 (1), 113–128.
- Tatsuoka, F., Koseki, J., Tateyama, M., Munaf, Y., Horii, N., 1998. Seismic stability against high seismic loads of geosynthetic-reinforced soil retaining structures. In: *Keynote Lecture, Proc. of the 6th Int. Conf. on Geosynthetics*, Atlanta, vol. 1, pp. 103–142.
- Tatsuoka, F., Tateyama, M., Murata, O., 1989. Earth retaining wall with a short geotextile and a rigid facing. In: *Proc. 12th Int. Conf. on SMFE*, Rio de Janeiro, pp. 1311–1314, 12(2).
- Tawfiq, K.S., Caliendo, J.A., 1993. Laboratory investigation of polyethylene sheeting as a friction reducer in deep foundations. *Geotext. Geomembr.* 12 (8), 739–762.
- Tognon, A.R., Rowe, R.K., Brachman, R.W.L., 1999. Evaluation of side wall friction for a buried pipe testing facility. *Geotext. Geomembr.* 17 (4), 193–212.
- Wu, C.S., Hong, Y.S., 2008. The behavior of a laminated reinforced granular column. *Geotext. Geomembr.* 26 (4), 302–316.
- Wu, C.S., Hong, Y.S., 2009. Laboratory tests on geosynthetics encapsulated sand columns. *Geotext. Geomembr.* 2 (2), 107–120.
- Wu, J.T.H., Ketchart, K., 2001. Performance Test for Geosynthetic Reinforced Soil Including Effects of Preloading. Report No. FHWA-RD-01-118. National Highway Institute, Federal Highway Administration, Washington, D.C.
- Wu, J.T.H., Pham, T., 2013. Load-carrying capacity and required reinforcement strength of closely spaced soil-geosynthetic composites. *J. Geotech. Geoenviron. Eng. ASCE* 139 (9), 1468–1476.
- Yang, K.H., Zornberg, J.G., Liu, C.N., Lin, H.D., 2012. Stress distribution and development within geosynthetic-reinforced soil slope. *Geosynth. Int.* 19 (1), 1–17.
- Zhang, M.X., Javadi, A.A., Min, X., 2006. Triaxial tests of sand reinforced with 3D inclusions. *Geotext. Geomembr.* 24 (4), 201–209.
- Zhang, M.X., Zhou, H., Javadi, A.A., Wang, Z.W., 2008. Experimental and theoretical investigation of strength of soil reinforced with multi-layer horizontal-vertical orthogonal elements. *Geotext. Geomembr.* 26 (1), 201–209.